

Towards Robust Medical Image Segmentation on Small-Scale Data with Incomplete Labels

Nanqing Dong, Michael Kampffmeyer, Xiaodan Liang, Min Xu, Irina Voiculescu,
and Eric P. Xing, *Fellow, IEEE*

Abstract—The data-driven nature of deep learning models for semantic segmentation requires a large number of pixel-level annotations. However, large-scale and fully labeled medical datasets are often unavailable for practical tasks. Recently, partially supervised methods have been proposed to utilize images with incomplete labels to mitigate the data scarcity problem in the medical domain. As an emerging research area, the breakthroughs made by existing methods rely on either large-scale data or complex model design, which makes them 1) less practical for certain real-life tasks and 2) less robust for small-scale data. It is time to step back and think about the robustness of partially supervised methods and how to maximally utilize small-scale and partially labeled data for medical image segmentation tasks. To bridge the methodological gaps in label-efficient deep learning with partial supervision, we propose RAMP, a simple yet efficient data augmentation framework for partially supervised medical image segmentation by exploiting the assumption that patients share anatomical similarities. We systematically evaluate RAMP and the previous methods in various controlled multi-structure segmentation tasks. Compared to the mainstream approaches, RAMP consistently improves the performance of traditional segmentation networks on small-scale partially labeled data and utilize additional image-wise weak annotations.

Index Terms—Partially Supervised Learning, Small Datasets, Robust Learning, Medical Image Segmentation

I. INTRODUCTION

Convolutional Neural Networks (CNNs) have been a game-changer for the task of semantic segmentation [1], [2], [3]. Unlike traditional segmentation methods, that rely on clustering, graph partitioning, and region growing approaches in combination with manual feature engineering, CNNs are able to learn a pixel-level mapping from the image space to the label space via end-to-end training. However, in order to learn these complex mappings, state-of-the-art CNNs usually leverage a large number of parameters and require the availability of large-scale fully labeled datasets. In the medical domain, where annotations require substantial efforts from the medical experts, obtaining these datasets can be challenging. Moreover,

the collection of clinical data has to take the law, privacy, and safety into consideration, which could incur additional costs. From the perspective of multi-task learning, a semantic segmentation task can be decomposed into multiple sub-tasks corresponding to each semantic class of interest. In a medical image segmentation task, a possible situation is that, for an image, the complete labels for all the sub-tasks are not available but incomplete (*partial*) labels for one or more sub-tasks are available. This situation is commonly caused by collecting and merging several smaller but relevant datasets into a larger dataset for the given task. These smaller datasets were originally labeled for sub-tasks, where only the objects related to the specific sub-task were annotated, while other objects were merged into the background. In other words, the training images do not have complete annotations for all classes of interest but are *partially labeled*. For example, in the task of abdominal organ segmentation, a pancreas dataset and a liver dataset might be available, where only the pancreas and the liver are labeled, respectively. Learning from partially labeled data, or *partially supervised learning* (PSL), is an open research question and has lately received increasing attention in medical image analysis [4], [5], [6], [7].

A key challenge, leading to poor segmentation performance when considering multiple partially labeled datasets, is that the semantic classes of one dataset could be categorized as background (BG) for another dataset that was annotated for a different purpose. Traditional semantic segmentation models [1], [2], [3] can therefore not be directly applied and trained end-to-end in a supervised fashion. Further, given the small partially labeled data and the huge number of parameters of deep learning models, CNNs will *memorize* [8] rather than *generalize* [9] from the data. Recent studies in PSL [4], [5], [6], [10], [7] all assume that, for each class of interest, enough training examples are accessible. However, considering the data scarcity in the practical medical tasks, usually, only a limited amount of training examples is available, making previous approaches impractical.

To bridge the methodological gaps when only limited partially labeled data is available, we tackle the problem by augmenting the partially labeled data. We propose a simple yet efficient framework RAMP, which can *robustly augment medical* data with *partial* labels. RAMP is designed to generate new training examples with complete labels. These examples allow us to transform the partially supervised problem into a fully supervised one. The proposed framework is motivated by vicinal risk minimization (VRM) [11], where new image-label pairs are drawn from a pre-defined vicinity distribution

N. Dong is with the Department of Computer Science, University of Oxford, Oxford, OX1 3QD, UK. (email: nanqing.dong@cs.ox.ac.uk)

M. Kampffmeyer is with the Department of Physics and Technology at the University of Tromsø, 9019 Tromsø, Norway.

X. Liang is with the School of Intelligent Systems Engineering, Sun Yat-sen University, Guangzhou, Guangdong 510006, China.

M. Xu is with the Computational Biology Department, Carnegie Mellon University, Pittsburgh, PA 15213, USA.

I. Voiculescu is with the Department of Computer Science, University of Oxford, Oxford, OX1 3QD, UK.

E. Xing is with the Machine Learning Department, Carnegie Mellon University, Pittsburgh, PA 15213, USA.

[11]. Recent studies have shown that VRM can consistently improve the performance of CNNs for image classification given appropriate vicinity distributions [12], [13]. However, there is a lack of definition of VRM for dense prediction tasks with incomplete labels. mixup [12] and CutMix [13] can not be directly applied on partially labeled images for multi-class segmentation tasks. In this work, we argue that data augmentation is a long-ignored but particularly efficient approach for medical image segmentation on small partially labeled datasets. RAMP defines a generic vicinity distribution for multi-structure segmentation based on the observation that the human structures, especially organs, show statistical similarities (e.g. shape, size, location) among different patients (see Fig. 1 for illustration of spatially aligned medical images.). We extensively investigate the properties of the proposed framework in various human structure segmentation tasks and illustrate that the proposed framework not only outperforms the baseline models by a large margin with limited data but also shows robustness under the challenges of class imbalance and domain shift.

To the best of our knowledge, this is the first systematic study of PSL under the challenge of data scarcity. The proposed framework has four advantages compared to previous methods: (1) it is easy to implement without complex loss function, network architecture, and optimization procedure, (2) it can be trained end-to-end in supervised settings with common segmentation networks and loss functions, (3) it does not require any fully labeled images in the training data, and (4) it can efficiently reduce the risk of overfitting when the size of training data is small.

Our main contributions can be summarized as follows:

- 1) We propose a robust framework for multi-structure segmentation for small datasets with partial supervision. The proposed framework neither requires large amounts of partially labeled images nor fully labeled images as a prior. The proposed framework can be applied to any end-to-end segmentation networks and loss functions.
- 2) We discuss the limitations of previous studies under the data scarcity challenge and the properties of the proposed framework in detail. Given a segmentation network, we show through extensive experiments that the proposed framework can consistently improve the segmentation performance compared to previous studies.
- 3) We extend the framework to scenarios when additional image-wise weak annotations are available.

II. RELATED WORKS

A. Semi-Supervised Learning

In the world of machine learning, semi-supervised learning (SSL) falls between supervised learning (SL), where only fully labeled training data are available, and unsupervised learning (UL), where no labels are available. In SSL, the training set consists of both labeled and unlabeled data. The robust and state-of-the-art SSL methods include label propagation (LP) [17], graph neural networks [18], [19], and adversarial training [20]. Among these seminal SSL methods, LP [21] can be applied to tackle partially labeled data directly. With

LP, pseudo-labels are generated based on prior information (partially labeled data). Then, the pseudo-labels are fine-tuned iteratively toward convergence [22]. LP is computationally expensive and the quality of the pseudo-labels is highly dependent on the number of training data. [6] has demonstrated that LP is a powerful solution to PSL with fully labeled datasets. As a robust method tested by time, LP is a strong baseline in this work. FocalMix [23] is a recently proposed SSL method to address medical object detection problems. Closely related to this work, FocalMix is also motivated by VRM. However, FocalMix is designed for object detection only and cannot handle partial labels.

B. Partially Supervised Learning

Closely related to SSL, partially supervised learning (PSL), or the partial labels problem, describes the situation where each example has an incomplete label (e.g. only one semantic class is annotated out of a few classes of interest). Concretely, given a collection of multiple small partially labeled datasets, each dataset may only contain annotations for a *proper subset* of classes of interest and these subsets are disjoint. In such a case, the images in the collection are partially labeled. A more rigorous formulation of the problem is presented in Section III-B.

PSL is a topic of active research as the perfect fully labeled training datasets tend to be only available for specific research tasks. In recent studies, several methods have been proposed to address semantic segmentation with partial labels from different aspects. Prior to the era of deep learning, [24] treats a grid of image patches as nodes and uses conditional random fields to propagate information. However, as a result, the predicted segmentation masks will be unnatural due to the patch-wise prediction. A common approach in deep learning is to treat the missing labels as the background. This approach can be viewed as a naive form of *noisy labels* [25] and only works when the pixels of missing classes take up a much smaller portion of the images, compared with the pixels of the BG. For benchmark datasets in computer vision such as PASCAL VOC [26] and MS COCO [27], there are only a few classes present in each image or the objects can be very small. Thus, merging unlabeled pixels into BG might be an efficient solution for these datasets. In contrast, for common medical datasets, multiple classes can be present in each image and the objects of interest (e.g. organs) may take up the majority of the pixels. Another common approach in deep learning is to ignore the cross entropy of the missing classes during the backpropagation [4], [5]. The limitation of this approach is that abandoning the pixel information of missing classes means that the learners (CNNs) will receive much less supervision during the learning process, both from the image space and the label space. A direct result is that the learner can not discriminate the classes of interest against BG. Recently, PaNN [6] proposes a complex Expectation-Maximization (EM) algorithm with a primal-dual optimization procedure. However, PaNN requires the availability of fully labeled images as prior, which is often unavailable. To address general semantic segmentation [26], [28], [10] proposes to use

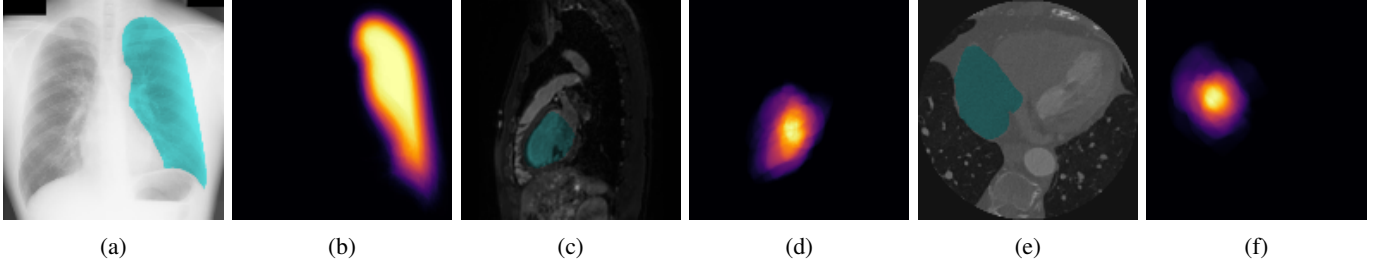


Fig. 1: (a) A posteroanterior X-ray image with the ground truth annotation of the left lung; (b) The label distribution (normalized density heatmap) of the left lungs in the JSRT dataset [14]; (c) A sagittal MRI image with the ground truth annotation of the left ventricle; (d) The label distribution of the left ventricles in the MRI-WHS dataset [15]; (e) An axial CT image with the ground truth annotation of the right atrium; (f) The label distribution of right atriums in the CT-WHS dataset [16].

a complex encoder-decoder architecture to condition the partial information within the CNN, which requires a large dataset to comply with the large number of parameters. PIPO-FAN [7] proposes a complex pyramid feature fusion mechanism and a target adaptive loss (TAL). Unlike the other methods, PIPO-FAN has a demanding requirement in the training process, i.e. the examples with the same partial labels must be trained together. It is worth mentioning that TAL also treats the missing labels as BG. To sum up, all of these methods are only applicable when substantial partially labeled images or fully labeled images are available. A detailed empirical analysis is provided in Section V-C.

C. Data Augmentation

Data augmentation is a common technique in machine learning to avoid overfitting and improve model performance. By creating altered copies of the training data, data augmentation can efficiently improve the generalization of deep learning models [29], especially when the training data is small or the training data is imbalanced in class distribution. Affine (or quasi-affine) transformations can almost be considered as a pre-processing routine in many computer vision tasks. Common operations include reflection, rotation, scaling, and translation of the images. Another popular method is adding some perturbation into the original distribution, e.g. altering the brightness and contrast of the original images, injecting Gaussian noise to the training images [30] and learning adversarial examples [31]. Interpolation-based methods interpolate the training data in linear or non-linear feature space [32]. Generative adversarial networks (GANs) [33] can also be used to generate new examples.

The data augmentation methods mentioned above have proven their efficiency in many SL tasks. However, these methods are less powerful in semantic segmentation with partial supervision. The original labels are only partial labels and the augmented labels are still only partial labels. Therefore these approaches do not solve the partial labels problem and the missing class information in the labels, which is the underlying problem, is still unaddressed. As a comparison, generating *noisy labels* can be viewed as a form of data augmentation. The missing labels are filled with pseudo-labels [34]. So the dataset is enlarged with more noisily labeled data. Here, the pseudo-labels are usually generated by knowledge transfer or

knowledge distillation based on the available information. As the extracted knowledge plays an important role in generating pseudo-labels, the knowledge transfer model can easily overfit to the small training data and lead to poor pseudo-labels. In fact, LP is one of these noisy labels methods.

D. Weakly Supervised Learning

Weakly supervised learning (WSL) defines the situation that only inaccurate or imprecise labels are available, e.g. pixel-wise labels are required for semantic segmentation while only coarse image-wise labels are available. Several approaches have been proposed to solve WSL in semantic segmentation from different perspectives, e.g. Bayesian methods [35], geometric methods [36], and GANs [37]. In Section III-D, we demonstrate how to extend RAMP with additional image-wise annotations. Unlike previous WSL methods, the proposed method focuses on the data generation process. See Section V-D3 for evaluation.

III. METHOD

A. Preliminaries

In SL, given a training dataset $S = \{X, Y\}$ with images $X = \{x_i\}_{i=1}^n$ and ground truth (GT) labels $Y = \{y_i\}_{i=1}^n$, the empirical risk is defined as

$$\mathcal{R}(h) = \frac{1}{n} \sum_{i=1}^n L(h(x_i), y_i), \quad (1)$$

where $L(\cdot, \cdot)$ is the loss function and $h \in \mathcal{H}$ is the hypothesis. In this work, we assume that L and h are universal as they can be any loss function and model in a standard supervised setting. For example, for a popular choice of semantic segmentation, L could be the cross entropy and h could be a CNN. The minimization of the empirical risk $\mathcal{R}(h)$ is also known as Empirical Risk Minimization (ERM) in statistical learning literature [38].

B. Problem Formulation

Assume there are $K > 1$ mutually exclusive semantic classes of interest, i.e. there is no hierarchical relationship between classes. In this work, we focus on the challenging situation that each image is annotated for only one semantic

class. For partially labeled images, we can always split S into K sub-datasets where each sub-dataset contains label information of only one class. Here, the K datasets are mutually exclusive in terms of both images and classes. Mathematically, we have $S = \bigcup_j^K S_j$, where $S_j = \{X_j, Y_j\}$ denotes the partially labeled dataset with label information of semantic class j . In S_j , $X_j = \{x_i^j\}_{i=1}^{n_j}$ is the image set of the images with label information of the semantic class j and $Y_j = \{y_i^j\}_{i=1}^{n_j}$ contains the corresponding partial labels.

Note, this is the most general case as all other cases are trivial extensions. For example, when an image has annotations for more than one semantic class, duplicate image copies could exist in multiple datasets and the above mathematical formulation still holds.

C. RAMP

RAMP is a data generation framework motivated by vicinal risk minimization (VRM) [11]. In VRM, a vicinity distribution \mathcal{V} is defined as the probability distribution for the virtual image-label pair (\tilde{x}, \tilde{y}) in the vicinity of (x, y) . The vicinal risk is defined as

$$\mathcal{R}_{\mathcal{V}}(h) = \frac{1}{n} \sum_i^n L(h(\tilde{x}_i), \tilde{y}_i). \quad (2)$$

In a fully supervised setting, adding Gaussian noise [11] and using the convex combination of the training data [12], [13] are two efficient methods to improve the robustness of deep learning models. However, as none of these methods can address the missing class information, they have been ignored in multi-class semantic segmentation with partial supervision for a long time. In this work, we integrate and extend these two simple ideas for medical image segmentation. Instead of designing complex networks or loss functions, we tackle the partial labels in the data generation process.

Based on the fact that human structures share statistical similarities [39], [40], [6], we propose a generic \mathcal{V} for the partially supervised problem in the medical domain, which can produce realistic (\tilde{x}, \tilde{y}) . Given (\tilde{x}, \tilde{y}) , we train the segmentation network by minimizing Eq. (2). From a Bayesian perspective, without any prior information on the true distribution, one of the common choices of prior is a uniform distribution, which maximally mixes the available information. Based on the same idea, we want to mix all the available partial labels.

Let x be a 2D medical image, which has been pre-processed via instance normalization and optional spatial alignment, and y be the corresponding partial label with one semantic class annotated. Each pixel of y is a $(K+1)$ -element one-hot vector for BG and K semantic classes. We use $y[k]$ to denote the binary label map for class $k \leq K$ ($k=0$ denotes BG), which is the $(k+1)^{th}$ channel of y . Let (x^j, y^j) be a random sample from S_j , and so $\{(x^j, y^j)\}_{j=1}^K$ is a K -element tuple of such samples. We define

$$\tilde{y} = \begin{cases} \frac{w_k y^k[k]}{\sum_{j=1}^K w_j y^j[j] + \epsilon} & k > 0 \\ 1 - \sum_{j=1}^K \tilde{y}[j] & k = 0 \end{cases} \quad (3)$$

$$\tilde{x} = \sum_{j=1}^K x^j \tilde{y}[j] + \frac{1}{K} \sum_{j=1}^K x^j \tilde{y}[0], \quad (4)$$

where all operations are element-wise, $w = (w_1, \dots, w_K) \sim \text{Dirichlet}(\alpha)$ with $\alpha \in (0, \infty)^K$ and $\epsilon > 0$ is a small number to ensure numeric stability, e.g. $\epsilon = 10^{-3}$.

See Fig. 2 for an illustration of the vicinal example generation. Additional to Fig. 2, we also show that the same K -element tuple can generate different vicinal examples generated based on $\text{Dirichlet}(\alpha)$ distribution in Fig.3.

Given fully labeled vicinal examples, without devising complex network architectures and loss functions, we can utilize the state-of-the-art segmentation networks [1], [2], [3] and common loss functions (e.g. cross entropy loss) in standard SL. An illustration of the complete training pipeline is provided in Fig. 4.

D. RAMP with Weak Annotations

The proposed framework can be extended when additional weak annotations are available. Compared with pixel-wise labels, image-wise labels (e.g. whether a certain organ or structure is present in an image) are referred to as weak annotations, and are much easier to acquire. We propose to utilize additional image-wise labels to alleviate the overgeneralization problem [41]. The overgeneralization phenomenon, originating in the field of domain adaptation, refers to the situation where the learner generalizes well in the source domain but performs poorly in the target domain. In our case, the training data generated by vicinal distribution can be viewed as the source domain and the real test data can be viewed as the target domain. From the view of statistical learning, we want to minimize the divergence between the vicinal training distribution \mathcal{V}_{train} and the real test distribution \mathcal{T}_{test} to decrease the empirical risk over the test set. RAMP could suffer from overgeneralization when we generate unrealistic vicinal examples.

Let C denote the number of classes actually contained in x (K is the number of total semantic classes). To maximally mix the available information, Eq. (3) and Eq. (4) assume that \tilde{x} contains all semantic classes ($C = K$ in Section III-C) by default. For example, a posteroanterior chest X-ray image should always include all the chest organs. However, in several medical imaging tasks, we have $C \leq K$ and C varies across images. For example, the size, the shape, and the location of organs vary across slices of CT or MRI scans even for the same patient. In Fig. 1, we can clearly see that the label density map of sagittal MRI images (Fig. 1(d)) and the label density map of axial CT images (Fig. 1(f)) show more uncertainty (more darkness in the boundary region of the organ) than the label density map of posteroanterior X-ray images (Fig. 1(b)). Let \mathcal{U}_C denote the set of semantic classes present in x and \mathcal{U}_K denote the set of all semantic classes of interest, we have $\mathcal{U}_C \subseteq \mathcal{U}_K$. According to Eq. (3) and Eq. (4), we sample K image-label pairs $(x^j, y^j)_{j=1}^K$ from $\bigcup_{j \in \mathcal{U}_C} S_j$ and $\bigcup_{j \in \mathcal{U}_K \setminus \mathcal{U}_C} S_j$. Note, the real image x does not contain the semantic classes in $\mathcal{U}_K \setminus \mathcal{U}_C$. In contrast, the vicinal examples will always contain all K semantic classes. That is to say, the non-parametric anatomical prior defined by Eq. (3) and Eq. (4) does not capture the real image and label distribution but introduces noise for the learner to generalize.

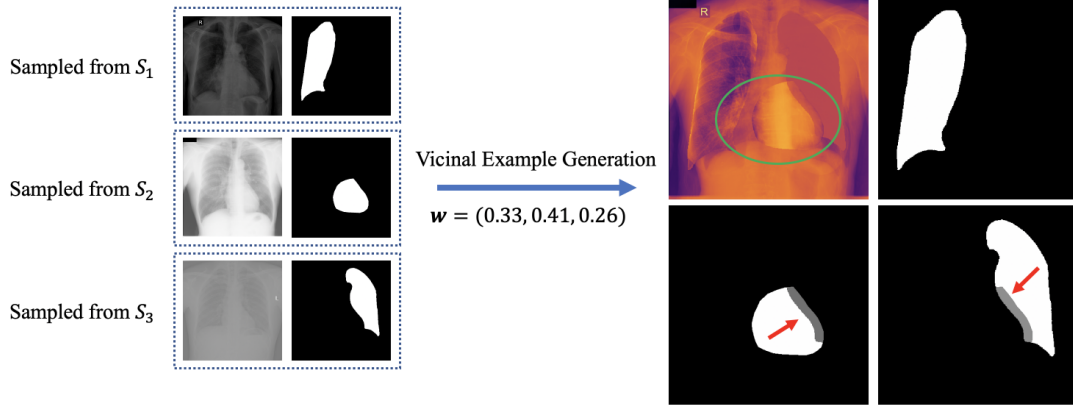


Fig. 2: Illustration of the vicinal example generation for chest organ segmentation. Three images with partial labels are sampled from three partially labeled datasets. Given randomly sampled w , normalized images and partial labels, we generate vicinal examples following Eq. (3) and Eq. (4). Here, spatial alignment is not required for this task as the imaging protocols for the chest localization are similar. The vicinal image is visualized by a density heatmap. The vicinal label is visualized per channel. In each channel, the continuous probabilities are transformed into grayscale pixels. Let us take a close look at the area within the green circle. When there is no overlap between partial labels, there is no obvious change to the original label (e.g. the partial label from S_1). When there is overlap, an uncertainty is introduced to the original label (e.g. the shaded regions pointed by the red arrows for the partial labels from S_2 and S_3).

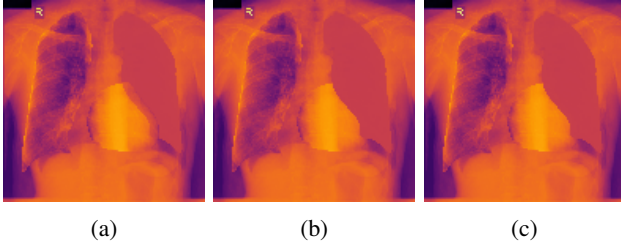


Fig. 3: Vicinal images (visualized by density heatmap) with the same input images in Fig. 2 but different w : (a) Uniform: $w = (\frac{1}{3}, \frac{1}{3}, \frac{1}{3})$, (b) Uni-modal: $w = (0.98, 0.01, 0.01)$, (c) Multi-modal: $w = (0.49, 0.49, 0.02)$.

We use the image-wise class information to *regularize* the data generation process. Assume that image-wise class labels for a subset of images S are available. We first randomly sample a base example pair from S . Without losing generality, we can assume that we have (x^j, y^j) , belonging to S_j . If the image-wise weak annotation \mathcal{C} is available for (x^j, y^j) , we sample (x^i, y^i) from S_i , $\forall i \in \mathcal{U}_C, i \neq j$ (as we already have (x^j, y^j)). For $i \notin \mathcal{U}_C$, we set $x^i = x^j$ and y^i to be a zero array. Again, we have a K -element tuple for Eq. (3) and Eq. (4). In case that x^j does not have a weak annotation, we perform the same sampling as described in Section III-C.

In practice, image-wise weak annotations can be acquired in many ways. For example, the clinicians can scribble or click the regions of interest in an interactive labeling system. For certain tasks, weak annotations could be inferred from medical knowledge or retrieved from the electronic health records.

IV. THEORETICAL ANALYSIS

In this section, we will discuss the motivation and the properties of the proposed framework.

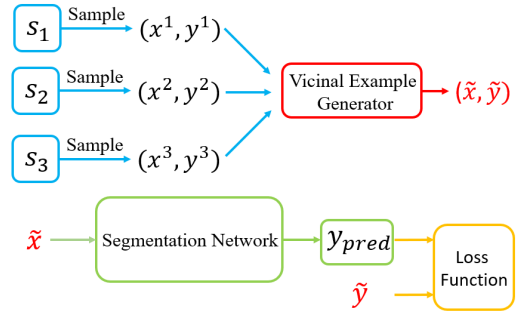


Fig. 4: Illustration of the complete training pipelines. Assume there are three partially labeled sub-datasets. $\{(x^1, y^1), (x^2, y^2), (x^3, y^3)\}$ are randomly sampled from S_1 , S_2 and S_3 . The vicinal generation process is depicted in Fig. 2. With (\tilde{x}, \tilde{y}) , the segmentation network is trained in a standard supervised setting.

A. Theoretical Motivation

The proposed method can be formulated as a problem that is closely related to domain adaptation, where the generated samples can be viewed as the source domain and the real test samples are the target domain. It has been proven that the domain adaptation performance is dominated by the discrepancy between the two domains [42]. In standard SL, we usually assume the training set and the test set sampled from the same population. However, this assumption may not be valid because of the data collection and generation process for PSL. Thus, designing a realistic vicinity distribution close to the real distribution is important in minimizing the target risk.

The proposed method utilizes the similarity assumption of human anatomical structures when the medical images

are spatially aligned (see Fig.1 for an intuitive illustration). For general objects or misaligned organs, RAMP can be still viewed as a form of data augmentation [12]. Eq. (3) and Eq. (4) indeed define non-parametric anatomical priors. Capturing priors has much more impact on medical images than on natural images [6]. However, without fully labeled training data, anatomical priors cannot be learned efficiently by previous methods [43], [44], [45]. In our definition, each $\tilde{y}[k]$ ($k > 0$) follows the label distribution of the corresponding structure k and \tilde{x} is a weighted average of $\{x^j\}_{j=1}^K$. Intuitively, for a real fully labeled pair (\hat{x}, \hat{y}) , we can obtain $\{(x^j, y^j)\}_{j=1}^K$ by setting $\{x^j = \hat{x}\}_{j=1}^K$ and decomposing the GT label \hat{y} into $\{y^j\}_{j=1}^K$. By applying Eq. (3) and Eq. (4) to $\{(x^j, y^j)\}_{j=1}^K$, (\tilde{x}, \tilde{y}) is a reconstruction of (\hat{x}, \hat{y}) subject to error ϵ .

For the interested readers, a more mathematical explanation of the motivation, from the perspective of the generalization bound, can be found in the Appendix.

B. Enlarged Sample Space

One of the main challenges for label-efficient deep learning is overfitting caused by data scarcity. In this work, there are two aspects of data scarcity: 1) each image has an incomplete label, and 2) each S_i has only a small number of images. For 1), Eq. (3) and Eq. (4) generate fully labeled vicinal examples where the features of the overlapped regions are the convex combination of original features in the same place. With fully labeled vicinal examples, traditional end-to-end training techniques in SL can finally be applied.

For 2), with limited training data, state-of-the-art CNN architectures can easily overfit the training data. Let us first isolate the randomness effect caused by the Dirichlet distribution by setting $w_i = \frac{1}{K}$. The proposed framework enlarges the sample space from $\sum_i n_i$ partially labeled examples to $\prod_i n_i$ fully labeled examples. In fact, with $\sum_i w_i = 1$, w can control the weight of each semantic class in the overlapped regions and enforce the discrete pixel value to lie in the range of $[0, 255]$. Given $\{(x_i, y_i)\}_{i=1}^K$, with w , we can theoretically generate an infinite number of different (\tilde{x}, \tilde{y}) . We efficiently mitigate the overfitting problem by enlarging the sample space of \tilde{S} .

C. Label Smoothing

In semantic segmentation tasks, labels usually follow a discrete distribution, while Eq. (3) defines a continuous distribution. Even though the application of continuous label distributions is rare in semantic segmentation, they have led to recent breakthroughs in image classification [46], [12]. We expect Eq. (3) can improve the robustness of the model as suggested by recent theoretical analysis of continuous label distribution [47].

D. Adversarial Training

Many breakthroughs have been made by adversarial training in medical image segmentation [48], [49], [50], [51]. However, adversarial training for semantic segmentation is ill-defined when GT labels are missing [52]. Following the alternative

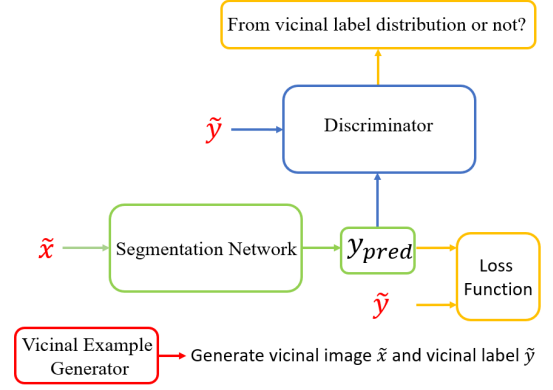


Fig. 5: Illustration of adversarial training pipeline for vicinal examples. (\tilde{x}, \tilde{y}) is generated by the vicinal example generator (Eq. 3 and Eq. 4). The segmentation network is trained with (\tilde{x}, \tilde{y}) in a supervised fashion. y_{pred} , the output of the segmentation network is the concatenation of $(K + 1)$ probability maps. An auxiliary discriminator is trained to identify whether y_{pred} is sampled from the vicinal distribution, i.e. discriminate y_{pred} against \tilde{y} . The segmentation network and the discriminator are trained alternatively. See Eq. 5 and Eq. 6 for details.

optimization procedure in [52], we train the segmentation network with an auxiliary discriminator. With (\tilde{x}, \tilde{y}) , the partially supervised task can be trained adversarially as a fully supervised task. The discriminator is used to align the prediction distribution and the label distribution [48], [39]. See Fig. 5 for the illustration of adversarial training with vicinal examples.

Assume the segmentation network is parameterized by f_θ and the discriminator is parameterized by g_ϕ . Given ϕ fixed, θ is updated by minimizing

$$L(\theta) = L_{seg}(f_\theta(\tilde{x}), \tilde{y}) - \lambda \log g_\phi(f_\theta(\tilde{x})), \quad (5)$$

where L_{seg} is the softmax cross-entropy and λ controls the weight of the adversarial loss. Given θ fixed, ϕ is updated by minimizing

$$L(\phi) = -\log g_\phi(\tilde{y}) - \log(1 - g_\phi(f_\theta(\tilde{x}))). \quad (6)$$

Further, *continuous* vicinal labels have a built-in advantage in stabilizing adversarial training. They alleviate the problem that there commonly is a clear discrepancy between the *discrete* distribution of the GT and the *continuous* distribution of the pixel-wise predictions, which can be easily caught by the discriminator [52] and destabilize training, leading to oscillating parameters [53].

E. Computational Cost

The training process of the proposed framework is identical to the training process for a fully supervised task, i.e. given a segmentation network, there is no additional optimization cost in backpropagation. Without introducing noisy labels, previous methods either suffer a longer training time [4] or have additional optimization targets [6]. Similarly, the proposed method

utilizes the same memory footprint in terms of CNN weights. As a comparison, a semi-supervised method such as knowledge transfer will require the training of multiple segmentation networks to generate pseudo-labels. For the proposed method, the major overheads arising from the data generation process are the random sampling and the element-wise operations on low-dimensional arrays which are negligible compared to the backpropagation cost. Eq. (3) and Eq. (4) can be easily implemented by any scientific computing frameworks supporting broadcasting, such as NumPy, TensorFlow, and PyTorch.

F. Limitations

The main purpose of the proposed framework is to enlarge the training set and train deep learning-based segmentation models in an efficient way. Instead of aiming to generate completely synthetic images, it instead aims to maximally utilize the existing data. Similar to GAN-based approaches, which have recently had a large impact in medical image applications, generated samples might introduce noise (see Section III-D) and should not be considered in line with the actual data.

As discussed in Section III-B, the design of Eq. (3) and Eq. (4) makes a strong assumption that there is no hierarchical relationship between the semantic classes, i.e. the classes of interest are mutually exclusive, e.g. organs in the same body part or sub-structures under the same structure. The situation where the semantic classes have a hierarchical structure, e.g. liver and liver tumor, is beyond the scope of discussion.

The proposed framework is designed for deep learning tasks on small datasets without fully labeled data. When fully labeled data is available, state-of-the-art SL methods and SSL methods have obvious advantages over the proposed framework. However, the proposed framework fills the gap when SL and SSL methods fail.

V. EXPERIMENTS

The purposes of the experimental design are twofold. First, there is no known systematic study of PSL with limited data. We also want to investigate the impact of limited partial labels on representative deep learning approaches and study the properties of the proposed framework in a controlled environment. Second, we want to empirically analyze the properties discussed in Section IV. That is to say, the experiments in this study are designed to highlight the limitations of previous methods and the advantages of RAMP.

We consider two segmentation tasks for images with different modalities, namely chest organ segmentation on posteroanterior chest X-ray images (CXRs) and whole heart segmentation on sagittal MRI images and axial CT images. For chest organ segmentation, all semantic classes are present in each image and the overlap among the label distributions of the organs is limited. Considering the relatively small complexity of the first task, we set up a controlled environment to observe the properties of the proposed framework. For whole heart segmentation, the semantic classes are not necessarily present in an image at the same time and there is more overlap

among the label distributions. We examine the efficiency of the proposed framework in a general situation and in a situation that additional image-wise weak annotations are available.

A. Datasets

JSRT The JSRT dataset, released by the Japanese Society of Radiological Technology (JSRT), is a benchmark dataset for chest organ segmentation [14]. JSRT contains 247 grayscale CXRs with pixel-wise annotations of the *left lung*, the *right lung*, and the *heart*. Each CXR has a size of 2048×2048 .

Wingspan The Wingspan dataset was collected by Wingspan Technology for the study of transfer learning and unsupervised domain adaptation in chest organ segmentation [39]. Wingspan contains 221 grayscale CXRs with pixel-wise annotations of left lung and right lung. The CXRs were collected from 6 hospitals with different imaging protocols. Wingspan expresses a large variety in the data modalities including brightness, contrast, position, and size.

MRI-WHS The MRI-WHS dataset [16] is a benchmark dataset in whole heart segmentation, which contains MRI scans for 20 patients. Each scan is represented as a 3D array and each slice of the scan is converted into a 2D image by mapping MRI intensity values to grayscale pixel values. MRI-WHS has manual segmentation of 7 substructures of the heart: the *left ventricle* blood cavity (LV), the *right ventricle* blood cavity (RV), the *left atrium* blood cavity (LA), the *right atrium* blood cavity (RA), the myocardium of the left ventricle, the ascending aorta, and the pulmonary artery. The image size and the number of slices per patients differ across patients. We use the sagittal view in this study.

CT-WHS The CT-WHS dataset [15] is a benchmark dataset in whole heart segmentation, which contains CT scans for 20 patients. Each scan is represented as a 3D array and each slice of the scan is converted to a 2D image by mapping Hounsfield units to grayscale pixel values. CT-WHS has manual segmentation of 7 substructures of the heart for 20 patients: LV, RV, LA, RA, the myocardium of the left ventricle, the ascending aorta, and the pulmonary artery. The image size and the number of slices per patients differ across patients. We use the axial view in this study.

B. General Implementation

The image size is fixed to be 512×512 . We pre-process the raw images by instance normalization. Given an image x , we obtain the normalized image \hat{x} by $\hat{x}^{ij} = \frac{x^{ij} - \mu(x)}{\sigma(x)}$, where (i, j) is the position of the pixel in a 512×512 image, and μ and σ are the mean and standard deviation of the pixels of x . In this study, we do not have any other pre-processing because there is no obvious difference in the relative position of objects in each image. In practice, when partially labeled datasets are acquired from different imaging protocols, pre-processing techniques such as registration, resizing, and cropping are necessary. There are no fully labeled images in the training set and we consider the setting where each training image only has an annotation of one semantic class, as described in Section III-B.

All experiments are implemented in TensorFlow on a NVIDIA Tesla K80. For a fair comparison, all the networks are initialized with the same random seed and trained from scratch. We use Adam [54], a gradient-based optimization, and standard multi-class cross entropy as the loss function in this work. The learning rate is 10^{-4} with a batch size 8 and the weight decay is 10^{-4} for all the experiments. The performance metric in this study is mean IOU (mIOU).

C. Chest Organ Segmentation

Chest organ segmentation is a benchmark task in medical image segmentation. We can easily control the environment to get an insight into the impact of the limited partial labels on various representative methods and the efficiency of RAMP. Without specification, the experimental comparison is conducted in such a way that different models use the same network backbone, loss function, training strategy, and the set of hyperparameters.

As the basic setting, we randomly choose 200 images from JSRT. We use 150 images to create 3 partially labeled datasets for left lung, right lung, and heart. Each dataset consists of 50 images and the annotations of the corresponding organ. We use the remaining 50 fully labeled images as the test set. In addition to the basic setting, we simulate three common scenarios in label-efficient deep learning. First, we want to examine how the size of the partially labeled dataset affects the model by including only η of the training images. To ensure that the networks receive approximately the same number of updates, we multiply the number of epochs by $\frac{1}{\eta}$. Second, we simulate the scenario of class imbalance. Because the heart is more difficult to annotate than the left lung and right lung [48], we only use 10% data of the heart dataset in the training for this scenario. Third, we simulate the scenario of multiple source domains, where each sub-dataset S_i represents a different source. The left lung and right lung datasets are sub-datasets of the Wingspan dataset, collected from different hospitals. The source for the heart is still the JSRT dataset. We consider three network architectures as the backbones, namely a ResNet18 [55] with bi-linear upsampling [3] (ResNet), a ResNet-based FCN-32s [1] (FCN), and a U-Net [2]. All the network backbones are identical to their original supervised settings. We include the performance of segmentation networks trained on the fully labeled data as an *Oracle* to provide a reference for the performance.

1) *Comparison with End-to-End Methods*: Among the previous studies on PSL, we consider two seminal end-to-end methods discussed in Section II-B as the baselines methods. The end-to-end methods are trained in a supervised fashion. The first one is mixing the missing classes with BG in the training, which can be considered as a naive solution with *noisy labels*. We denote the first baseline as MBG. The second baseline is ignoring the cross entropy of the missing classes during the backpropagation, denoted as IMBP. It is worth mentioning that MBG and IMBP are the foundations of many recent methods for the partial labels problem [4], [5], [7].

The results are shown in Table I. Note, the networks trained by RAMP consistently outperform their counterparts in all the

scenarios. Without a large number of partial labels, benchmark segmentation models such as FCN and U-Net become less useful when they are trained without RAMP. Take U-Net as an example, MBG has better performance with small η than with large η , because more examples introduce more noise. In contrast, although IMBP tends to achieve better performance with more data, ignoring the information of the missing classes makes the networks receive visual signals from particular regions instead of the whole images. The results also validate our hypothesis that RAMP is efficient when the “uniform prior” assumption is correct.

To highlight the limitations of the previous end-to-end methods, we provide a qualitative comparison in Fig. 6. It can be seen that when the data is small (small η), MBG predicts most of the region as BG because the classes of interest take up the majority of pixels. For the same reason, IMBP cannot properly identify BG as it abandons BG information during the optimization, which validates the discussion in Section II-B. Note, the results displayed in this section are implemented with the same network backbone and loss function. There are recent studies [5], [7] that proposes complex network architectures and loss functions based on MBG and IMBP, which are discussed in Section V-C3.

2) *Comparison with Transfer Learning Methods*: Another family of methods that require less labeled training data compared to the end-to-end approaches utilize knowledge transfer between the partially labeled datasets. These transfer learning methods are trained in a semi-supervised fashion and we consider the following three baselines. The first baseline is naive transfer learning (TL), which trains K binary segmentation networks on the labeled organs and predicts on the test set. In this work, we fuse the K binary predictions based on the maximum out of the K probabilities. If the maximum is less than 0.5, the pixel is predicted as BG. The second baseline is label propagation (LP). Similar to TL, LP is not an end-to-end method as there are multiple training stages. We first generate pseudo-labels for unlabeled organs in the training set by TL. The quality of noisy pseudo-labels is dependent on the training of the K binary segmentation networks. Then the pseudo-labels and GT labels are trained together to make a final prediction [6]. The third baseline is transfer learning with shared network backbone (TL-S). K binary segmentation networks share the same network backbone (e.g. ResNet) and have independent last layers. We alternatively optimize K binary segmentation networks on the corresponding K partially labeled datasets.

Note that SSL models usually require more memory space to train multiple models and they are sensitive to the size of the available training set. Because K binary segmentation networks are trained separately, TL, LP, and TL-S, are prone to overfitting with class imbalance and domain shift. U-Net has more parameters and structural advantages than FCN and with enough fully labeled training data it should outperform the FCN. However, for small datasets, overfitting is a serious problem and U-Net does have worse performance when η is small in Table I. For transfer learning tasks, especially with domain shift, FCN appears less prone to overfit with dataset shift than U-Net (with less parameters), and is therefore used

| Method | $\eta = 10\%$ | $\eta = 20\%$ | $\eta = 50\%$ | $\eta = 100\%$ | Imbalanced | Multiple Sources |
|---|---------------|---------------|---------------|----------------|------------|------------------|
| MBG + ResNet | 0.385 | 0.322 | 0.293 | 0.249 | 0.298 | 0.228 |
| MBG + FCN | 0.249 | 0.317 | 0.373 | 0.459 | 0.411 | 0.337 |
| MBG + U-Net | 0.402 | 0.312 | 0.091 | 0.111 | 0.436 | 0.265 |
| IMBP + ResNet | 0.375 | 0.386 | 0.445 | 0.433 | 0.413 | 0.430 |
| IMBP + FCN | 0.311 | 0.320 | 0.389 | 0.393 | 0.358 | 0.375 |
| IMBP + U-Net | 0.293 | 0.408 | 0.423 | 0.414 | 0.265 | 0.414 |
| RAMP + ResNet ($\alpha = 0.1$) | 0.795 | 0.826 | 0.832 | 0.843 | 0.838 | 0.771 |
| RAMP + FCN ($\alpha = 0.1$) | 0.787 | 0.811 | 0.829 | 0.834 | 0.836 | 0.783 |
| RAMP + U-Net ($\alpha = 0.1$) | 0.775 | 0.822 | 0.840 | 0.856 | 0.838 | 0.784 |
| RAMP + ResNet ($\alpha \rightarrow \infty$) | 0.780 | 0.801 | 0.821 | 0.849 | 0.751 | 0.801 |
| RAMP + FCN ($\alpha \rightarrow \infty$) | 0.788 | 0.821 | 0.850 | 0.860 | 0.826 | 0.815 |
| RAMP + U-Net ($\alpha \rightarrow \infty$) | 0.785 | 0.847 | 0.873 | 0.878 | 0.855 | 0.840 |
| <i>Oracle</i> + ResNet | 0.860 | 0.865 | 0.883 | 0.901 | 0.821 | 0.804 |
| <i>Oracle</i> + FCN | 0.868 | 0.895 | 0.913 | 0.921 | 0.907 | 0.817 |
| <i>Oracle</i> + U-Net | 0.861 | 0.890 | 0.917 | 0.923 | 0.908 | 0.842 |

TABLE I: mIOU of End-to-end Methods for Chest Organ Segmentation. RAMP outperforms other baseline methods and is close in performance to the *Oracle* methods with access to full labels.

to provide a more straight-forward comparison between the proposed method and other baselines. Here, we report the best performance of TL, LP, TL-S, RAMP ($\alpha = 0.1$), and *Oracle* for FCN initialized with the same random seed in Table II.

Although, the performance of TL-S is slightly better than TL, both TL and TL-S suffer from overfitting due to the small datasets, class imbalance and domain shift. Note, RAMP can train the model on more (generated) examples and does not require training of multiple network heads (the last layers), thus outperforming the TL and TL-S baselines.

Similarly, we provide a qualitative comparison between RAMP and LP in Fig. 6. As discussed in Section II-A, LP is a computationally expensive method and struggles when the available data is small. In fact, SSL methods usually need to rely on a large amount of unlabeled data (partially labeled data in our case). Although both RAMP and LP can roughly segment the organs of interest, RAMP apparently produces smoother boundaries than LP. A hypothesis here is that when data is small, the quality of the pseudo labels can not be guaranteed. It is worth mentioning that in recent studies in PSL [6], [10], [7], SSL methods have been ignored. A direct implication from this section is that with enough partially labeled data, SSL methods can achieve comparable performance with PSL methods.

3) *Comparison with State-of-the-Art Methods*: For a fair quantitative comparison, the above experiments are conducted in a controlled fashion. In this section, a comparative analysis is provided between RAMP and state-of-the-art methods. As state-of-the-art methods all have complex network architectures, we use U-Net as the backbone for RAMP ($\alpha = 0.1$) and *Oracle*. The results are present in Table III.

SMILE [5] can be viewed as an extension of IMBP. SMILE uses DeepLab (ResNet 101) [3] as the feature extractor and K independent binary (pixel-wise) classifier for each class of interest. SMILE uses a weighted methodology to fuse the information from K classes and the weights can also be used to filter out ambiguous BG, which can alleviate the missing BG phenomenon in Fig. 6. The K cross-entropy loss are summed as the final loss in the optimization.

PIPO-FAN [7] is a strong baseline model. PIPO-FAN proposes a U-Net based pyramid feature fusion method and

target adaptive loss. Similar to MBG, PIPO-FAN also treats the missing labels as BG*. Compared with other end-to-end methods, one huge difference in training strategy for PIPO-FAN is that PIPO-FAN has to be trained on each sub-dataset one by one. In contrast, most end-to-end methods with stochastic gradient descent (SGD) optimization have random samples in each batch. It is also worth mentioning that, PIPO-FAN takes around 5 times longer to converge during training than RAMP and *Oracle*.

Another related work not included in Table III is PaNN [6]. PaNN can be considered as an extension to LP, which generates pseudo labels by learning an image prior from fully labeled data. Instead of using SGD, PaNN uses an Expectation-Maximization algorithm with primal-dual optimization. A critical restriction for PaNN is that fully labeled data must be available. Here, we provide the result of LP in Table III as a reference.

As a short conclusion for the experiments between RAMP and previous methods, data augmentation is an efficient and robust approach in terms of computational cost and performance when the dataset is small.

4) *Impact of Network Complexity*: Even though RAMP can efficiently utilize the available data, the complexity of the segmentation network still plays an important role. The network complexity is determined by the number of parameters and the network architecture. For supervised tasks, U-Net should outperform FCN and ResNet because U-Net (38.8M) has more parameters than FCN (13.3M) and ResNet (11.2M) and a better network architecture design for segmentation tasks. Clearly, there is a trade-off in the model selection between model complexity and model performance when the partially labeled data is small (e.g. $\eta = 10\%$). A similar phenomenon can also be found in MBG and IMBP. We infer that high network complexity could exacerbate the overfitting problem for partially labeled data with a small sample size.

5) *Impact of Classical Data Augmentation*: We also perform a comparative experiment with additional data augmentation (DA) for the baseline methods. The additional data augmentation includes random rotation (90° , 180° , 270°), random

*The implementation of PIPO-FAN can be found at <https://github.com/DIAL-RPI/PIPO-FAN>.

| Method | $\eta = 10\%$ | $\eta = 20\%$ | $\eta = 50\%$ | $\eta = 100\%$ | Imbalanced | Multiple Sources |
|---------------|---------------|---------------|---------------|----------------|------------|------------------|
| TL | 0.651 | 0.743 | 0.761 | 0.790 | 0.695 | 0.550 |
| LP | 0.701 | 0.765 | 0.789 | 0.814 | 0.710 | 0.684 |
| TL-S | 0.692 | 0.773 | 0.787 | 0.803 | 0.701 | 0.581 |
| RAMP | 0.787 | 0.811 | 0.829 | 0.834 | 0.836 | 0.783 |
| <i>Oracle</i> | 0.868 | 0.895 | 0.913 | 0.921 | 0.907 | 0.817 |

TABLE II: Comparison with transfer learning methods. FCN is the network backbone for all methods. We set $\alpha = 0.1$ for RAMP.

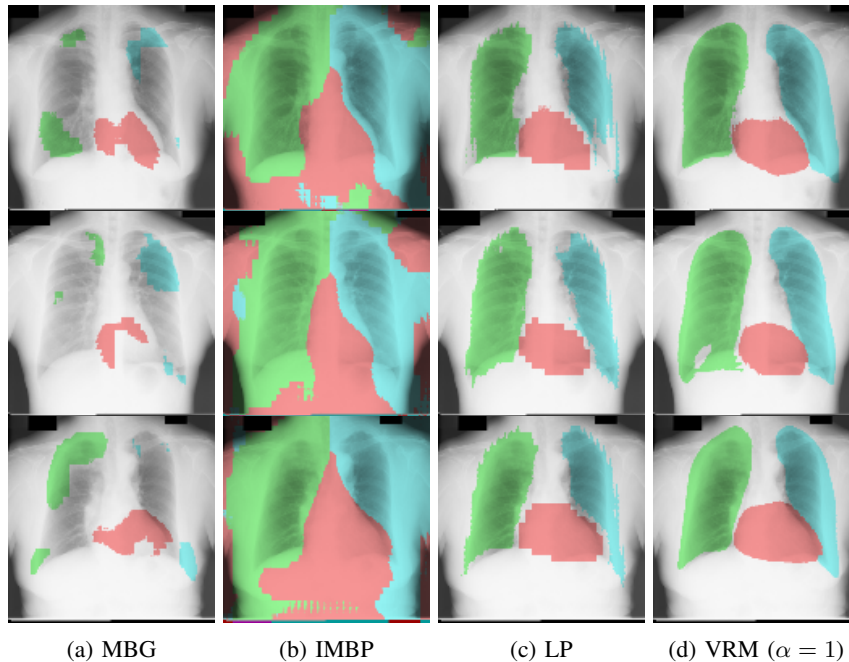


Fig. 6: Qualitative comparison on chest organ segmentation task with $\eta = 10\%$. The network bone is FCN. The training details are described in the corresponding sections.

| Method | $\eta = 10\%$ | $\eta = 20\%$ | $\eta = 50\%$ | $\eta = 100\%$ | Imbalanced | Multiple Sources |
|---------------|---------------|---------------|---------------|----------------|------------|------------------|
| SMILE [5] | 0.643 | 0.715 | 0.766 | 0.792 | 0.694 | 0.560 |
| PIPO-FAN [7] | 0.705 | 0.773 | 0.787 | 0.825 | 0.777 | 0.695 |
| LP | 0.701 | 0.765 | 0.789 | 0.814 | 0.710 | 0.684 |
| RAMP | 0.775 | 0.822 | 0.840 | 0.856 | 0.838 | 0.784 |
| <i>Oracle</i> | 0.861 | 0.890 | 0.917 | 0.923 | 0.908 | 0.842 |

TABLE III: Comparison with state-of-the-art methods. U-Net is the network bone for RAMP ($\alpha = 0.1$) and *Oracle*.

horizontal flipping, and color jittering (brightness only). Here, the color jittering is implemented by adding Gaussian noise after the instance normalization. In this experiment, for the same reason in Section V-C2, we use FCN as the backbone to avoid overfitting. The data augmentation for end-to-end baseline methods is straight-forward, following standard SL procedures. For transfer learning methods with multiple stages, data augmentation is performed across the whole training process. We report RAMP with $\alpha = 0.1$, without any data augmentation.

As discussed in Section II-C, classical data augmentation does not address partial labels problem directly. In contrast, RAMP generates fully labeled vicinal examples. The results are shown in Table IV. Classical data augmentation has limited effect on the baseline methods. Among baseline methods, transfer learning methods benefit more from data augmentation than end-to-end methods.

6) *Sensitivity of α* : In Table I, we include the results of two representative values of α , a small one ($\alpha = 0.1$) and an extreme large one ($\alpha \rightarrow \infty$). Dirichlet(α) is asymptotically close to a uniform distribution when $\alpha \rightarrow \infty$, i.e. $w_i = \frac{1}{K}$. The performance of a ResNet trained by RAMP with different α is shown in Fig. 7. There is a trade-off in selecting the optimal α . Given $C = K$ for every image, we can infer that a small α works well for small sample size while a moderately large α works well for large sample size.

The problem becomes much more complicated if C depends on the image (as discussed in Section III-D). First, extra caution should be paid to K as α is sensitive to K . Intuitively, as $K \rightarrow \infty$, the features of overlapped regions will be completely smoothed out. Second, there will be a severe overgeneralization phenomenon when the assumption of “uniform prior” is wrong. A large α will strengthen this wrong assumption, thus worsen the overgeneralization phenomenon. Without loss of

| Method | $\eta = 10\%$ | $\eta = 20\%$ | $\eta = 50\%$ | $\eta = 100\%$ | Imbalanced | Multiple Sources |
|---------------|---------------|---------------|---------------|----------------|------------|------------------|
| MBG + DA | 0.252 | 0.319 | 0.376 | 0.460 | 0.414 | 0.341 |
| IMBP + DA | 0.314 | 0.321 | 0.391 | 0.395 | 0.359 | 0.377 |
| TL + DA | 0.659 | 0.747 | 0.764 | 0.794 | 0.695 | 0.550 |
| LP + DA | 0.705 | 0.767 | 0.792 | 0.819 | 0.715 | 0.689 |
| TL-S + DA | 0.696 | 0.780 | 0.791 | 0.809 | 0.710 | 0.585 |
| RAMP | 0.787 | 0.811 | 0.829 | 0.834 | 0.836 | 0.783 |
| <i>Oracle</i> | 0.868 | 0.895 | 0.913 | 0.921 | 0.907 | 0.817 |

TABLE IV: Impact with additional data augmentation. FCN is the network backbone for all methods. RAMP ($\alpha = 0.1$) does not have additional data augmentation.

generality, we restrict $\alpha \leq 1$ in practice.

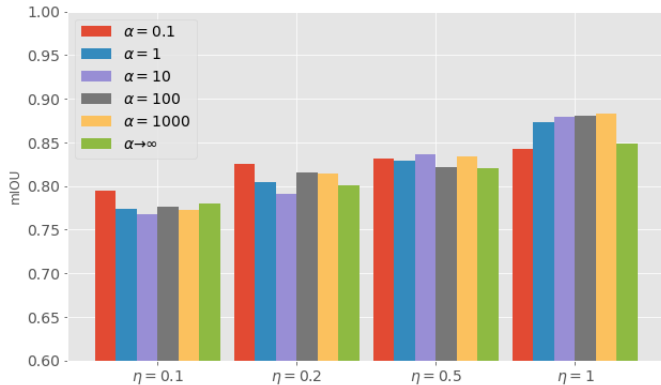


Fig. 7: Sensitivity of α to η

7) *Adversarial Training*: In RAMP with adversarial training (ADV), there is an auxiliary discriminator trained jointly with the segmentation network. A large variety in sample space (i.e. small α) requires a delicate design of the discriminator to learn the high-order statistics of the label distribution [41] as the training system could be sabotaged by an inappropriate discriminator [40]. For adversarial training, the choice of the discriminator is a research question in its own right. The discriminator is usually chosen to have the same backbone as the segmentation network to increase the stability of adversarial training [56]. We therefore use a ResNet-based FCN with a standard ResNet discriminator in order to improve performance and convergence. Here, we adopt an alternative optimization scheme following the adversarial training procedure described in [52], [48], [39], where the adversarial loss [52] in Eq. (5) is weighted by $\lambda = 0.001$. To illustrate the effect of ADV alone, we use a uniform distribution ($\alpha \rightarrow \infty$) to minimize the effect of data augmentation caused by small α . We report the results of RAMP with and without adversarial training in Table V.

When η decreases, ADV tends to close the gap between the performance of fully labeled training and partially labeled training even with an extremely large α . We conclude that ADV can be used as an add-on module for RAMP with *appropriate* α and *delicate* design of the network architecture for the discriminator.

D. Whole Heart Segmentation

With a basic understanding of the properties of RAMP from Section V-C, we evaluate RAMP on the task of whole

heart segmentation. Compared with chest organ segmentation, whole heart segmentation is a more difficult and practical task. As discussed in Section III-D, the categories of organs present in different slices of the same patient could be completely different. In addition, there is a massive overlap among the label distributions of the semantic classes for whole heart segmentation. We want to test the robustness of RAMP under these new challenges. Meanwhile, following Section V-C, we aim to understand the limitations of mainstream PSL methods under these new challenges and the experiments within this section are therefore conducted in a controlled fashion. Based on the findings in Section V-C, we choose $\alpha = 0.1$ and use FCN as the segmentation network for all frameworks. We report both mIOU and individual IOU for each semantic class. Note, in this study, we explore a general data augmentation approach for PSL, which could be combined with alternative advances that focus on the design of advanced network architectures [5], [7], optimization procedures [6], or loss functions [7].

1) *Results on MRI-WHS*: For MRI-WHS, we choose LV, RV, and LA, which are three major classes in whole heart segmentation, as the classes of interest. We create partially labeled datasets where each dataset contains MRI images of a patient from MM-WHS. The images with only BG are removed. For the training set, we have 58 images for LV, 64 images for RV, and 75 images for LA. The test set consists of 450 images sampled from the other patients. The results are reported in Table VI. RAMP consistently outperforms the baseline methods by a large margin in both mIOU and individual IOU for each semantic class.

2) *Results on CT-WHS*: For axial CT scans, the labeled images are usually expected to include as many slices as possible per patient to learn the geometric variety of the structure along the axial axis. In this experiment, we further decrease the size of each partially labeled datasets. For each partially labeled dataset, we randomly choose approximately 1/3 of the total slices of a patient. In CT-WHS, we choose four classes of interest, which are LV, RV, LA, and RA. The images with only BG are removed. For the training set, we have 37 images for LV, 49 images for RV, 29 images for LA, and 44 images for RA. The test set consists of 496 images sampled from the other patients. The results are reported in Table VII. Similar to the results for MRI-WHS, RAMP is also efficient for this scenario when compared to the baseline approaches.

3) *RAMP with Additional Weak Annotations*: In this experiment, we simulate the situation that additional image-wise labels are available. In a real situation, the annotator can easily

| Backbone | Method | $\eta = 10\%$ | $\eta = 20\%$ | $\eta = 50\%$ | $\eta = 100\%$ |
|----------|---------------|---------------|---------------|---------------|----------------|
| ResNet | Vanilla | 0.795 | 0.826 | 0.832 | 0.843 |
| | ADV | 0.810 | 0.835 | 0.847 | 0.858 |
| | <i>Oracle</i> | 0.849 | 0.890 | 0.914 | 0.918 |
| FCN | Vanilla | 0.787 | 0.811 | 0.829 | 0.834 |
| | ADV | 0.808 | 0.830 | 0.851 | 0.877 |
| | <i>Oracle</i> | 0.868 | 0.895 | 0.913 | 0.924 |

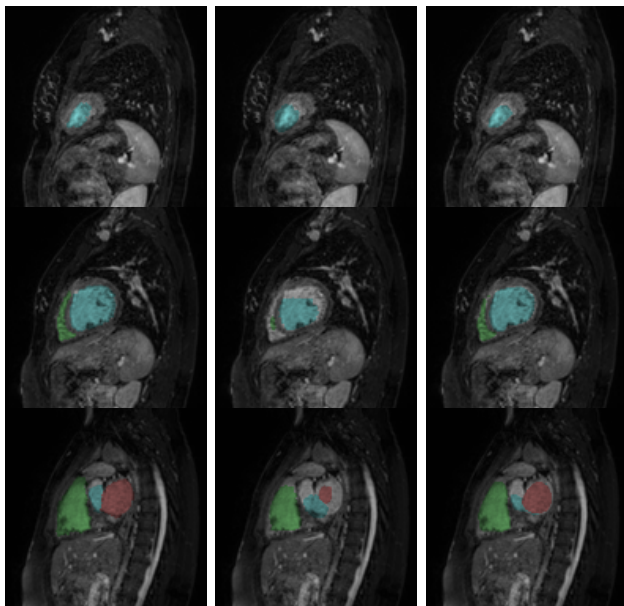
TABLE V: mIOU for RAMP with Adversarial Training

| Method | LV | RV | LA | mIOU |
|---------------|-------|-------|-------|-------|
| MBG | 0.164 | 0.028 | 0.142 | 0.111 |
| IMBP | 0.007 | 0.080 | 0.026 | 0.038 |
| TL | 0.171 | 0.147 | 0.152 | 0.157 |
| LP | 0.206 | 0.179 | 0.181 | 0.189 |
| TL | 0.192 | 0.163 | 0.183 | 0.179 |
| RAMP | 0.283 | 0.205 | 0.285 | 0.258 |
| RAMP+ | 0.433 | 0.230 | 0.285 | 0.316 |
| <i>Oracle</i> | 0.502 | 0.439 | 0.428 | 0.456 |

TABLE VI: Results for Whole Heart Segmentation on MRI-WHS

| Method | LV | RV | LA | RA | mIOU |
|---------------|-------|-------|-------|-------|-------|
| MBG | 0.108 | 0.000 | 0.298 | 0.000 | 0.102 |
| IMBP | 0.027 | 0.026 | 0.087 | 0.013 | 0.038 |
| TL | 0.237 | 0.183 | 0.363 | 0.287 | 0.268 |
| LP | 0.303 | 0.214 | 0.425 | 0.323 | 0.316 |
| TL-S | 0.267 | 0.223 | 0.374 | 0.288 | 0.288 |
| RAMP | 0.333 | 0.277 | 0.531 | 0.408 | 0.387 |
| RAMP+ | 0.356 | 0.396 | 0.575 | 0.415 | 0.435 |
| <i>Oracle</i> | 0.429 | 0.504 | 0.600 | 0.599 | 0.533 |

TABLE VII: Results for Whole Heart Segmentation on CT-WHS

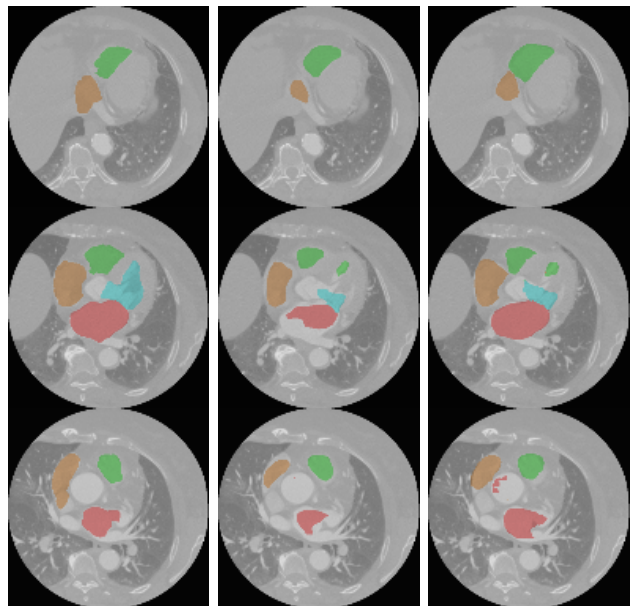


(a) GT

(b) VRM

(c) VRM+

Fig. 8: Visualization for Whole Heart Segmentation on MRI-WHS.



(a) GT

(b) VRM

(c) VRM+

Fig. 9: Visualization for Whole Heart Segmentation on CT-WHS.

tell whether a certain organ is present in an image with just a glimpse. Thus, image-wise labels can be obtained at only a fraction of the cost of pixel-wise annotations. We simulate this process by inferring the image-wise labels directly from the original complete pixel-wise ground truth labels (not the

partial labels) where all organs are annotated. The training procedure is updated as described in Section III-D. Here, the image-wise labels for the classes of interest are represented as K -element binary vectors. We denote RAMP with additional weak annotation as RAMP+. The results are reported in

Table VI and Table VII. We can see that the “uniform prior” assumption of RAMP tends to cause overgeneralization when a structure is largely overlapped with other structures, e.g. LV is the largest structure in terms of size in this experiment. The additional weak annotation can efficiently mitigate the problem. The visual difference between RAMP and RAMP+ can be easily spotted in Fig. 8 and Fig. 9.

E. Data-Dependent Performance

Based on the above experiments, we observe that the quality of vicinal distribution \mathcal{V} tends to be influenced by the variety in the shape, the size, and the location of the organs in the real distribution \mathcal{S} . Considering that human structures share statistical similarities, we hypothesize that a small variance in the real label distributions leads to a realistic vicinal label distribution, with a small distributional discrepancy between \mathcal{V} and \mathcal{S} . Similarly, we can imagine that a large variance could lead to an unrealistic vicinal label distribution with a large distributional discrepancy.

In Section V-C, the performance on the dataset with multiple sources is always lower than the performance on the dataset collected from a single source. Intuitively, the dataset shift could also be interpreted as a large variance in \mathcal{S} . Now we take Section V-C and Section V-D as two tasks (two different real distributions) for an overall comparison. Although RAMP can outperform the baseline methods with the same experimental setup, RAMP apparently achieves lower performance in the second task. As we discussed in Section III-D, this is due to the fact that the second task has a much larger uncertainty (variance in distribution). We can conclude that the quality of the vicinal distribution and the performance of RAMP are intrinsically determined by \mathcal{S} .

VI. FUTURE WORK

In this work, the proposed framework focuses on 2D segmentation. Theoretically, RAMP can be extended to 3D multi-structure segmentation with the help of 3D CNNs [57]. For volumetric medical images, there are four dimensions, including height, width, length, and one-hot encoded class channel. Following the same similarity assumption and VRM motivation, if we now consider x^j as a 3D image and y^j as the corresponding partial labels (3D because the class channel is only a binary map instead of one-hot encoded), Eq. 3 and Eq. 4 still hold with proper adaptation. The generated vicinal example (\tilde{x}, \tilde{y}) is fully labeled for 3D CNNs.

Note, 3D CNNs are much more computationally expensive than 2D CNNs due to 3D convolution operations. With a large number of parameters and a small number of partially labeled 3D images, RAMP is expected to mitigate the data scarcity issue and achieve robust performance. The detailed discussion and implementation of 3D medical image segmentation are beyond the scope of this paper, thus left as future work.

VII. CONCLUSION

In this paper, we discuss the robustness issue of PSL methods under the challenge of data scarcity. We present RAMP, an easy-to-implement framework, that can efficiently utilize small

partially labeled data for multi-structure segmentation. We analyze the properties of RAMP and evaluate it under various practical scenarios. RAMP is robust under various extreme situations and outperforms all the other PSL methods with small datasets. Our research suggests a new research direction in label-efficient deep learning with partial supervision.

APPENDIX A

THEORETICAL MOTIVATION

Let us denote the generated distribution of $\tilde{S} = \{\tilde{X}, \tilde{Y}\}$ as \mathcal{S} and the target distribution of T as \mathcal{T} . Building on classical generalization bounds from domain adaptation, the following theorem holds:

Theorem 1 (Generalization Bound). *With probability $1 - \delta$ over the choice of n samples \tilde{S} from \mathcal{S} and T from \mathcal{T} , for $h \in \mathcal{H}$ of VC dimension d :*

$$\begin{aligned} \mathcal{R}_{\mathcal{T}}(h) \leq & \mathcal{R}_{\mathcal{V}}(h) + \sqrt{\frac{4}{n} \left(d \log \frac{2en}{d} + \log \frac{4}{\delta} \right)} \\ & + 4 \sqrt{\frac{1}{n} \left(d \log \frac{2n}{d} + \log \frac{4}{\delta} \right)} + \hat{d}_{\mathcal{H}}(\tilde{S}, T) \\ & + \Omega(\mathcal{S}, \mathcal{T}, \mathcal{H}), \end{aligned} \quad (7)$$

where $\hat{d}_{\mathcal{H}}(\tilde{S}, T)$ is a distance between \tilde{S} and T , and $\Omega(\mathcal{S}, \mathcal{T}, \mathcal{H}) \geq \inf_{h^* \in \mathcal{H}} [\mathcal{R}_{\mathcal{S}}(h^*) + \mathcal{R}_{\mathcal{T}}(h^*)]$ is the lower bound for the sum of the risk \mathcal{R} on \mathcal{S} and \mathcal{T} .

Proof. (Sketch) If we take \mathcal{S} as the source domain of \tilde{S} and \mathcal{T} as the target domain of T , the partial supervision problem for VRM can be transformed into a domain adaptation problem.

Assume there is a fully labeled training dataset S' which shares the same X as the partially labeled S . We consider \mathcal{H} as a set of binary classifiers for simplicity, i.e. $h : x \mapsto \{0, 1\}$. Following [42], with a standard application of VC theory [38], we can get

$$\mathcal{R}_{\mathcal{T}}(h) \leq \mathcal{R}_{S'}(h) + \sqrt{\frac{4}{n} \left(d \log \frac{2en}{d} + \log \frac{4}{\delta} \right)} + d_{\mathcal{H}}(S', T) + \lambda, \quad (8)$$

where $d_{\mathcal{H}}(S', T) = 2 \sup_{H \in \mathcal{H}} |P_{S'}(H) - P_T(H)|$ is the \mathcal{A} -distance [58] and λ means the hypothesis h is λ -close to \mathcal{H} for the distributions of S' and T . In practice, the \mathcal{A} -distance can be approximated by proxy \mathcal{A} -distance $\hat{d}_{\mathcal{H}}(S', T)$ [42].

For vicinal dataset \tilde{S} , it is natural to have $\mathcal{R}_{\mathcal{V}}(h) > \mathcal{R}_{S'}(h)$. Because $\hat{d}_{\mathcal{H}}(S', T)$ and $\hat{d}_{\mathcal{H}}(\tilde{S}, T)$ are measurement on the distributional similarities, so these two terms do not involve any true labels. When the similarity assumption holds, we have $\hat{d}_{\mathcal{H}}(\tilde{S}, T) \geq \hat{d}_{\mathcal{H}}(S', T)$. This means that $\hat{d}_{\mathcal{H}}(S', T)$ can be replaced with $\hat{d}_{\mathcal{H}}(\tilde{S}, T)$. By definition, partially labeled S and unlabeled T are both accessible by \mathcal{H} . We apply Theorem 2 of [42] because the true labels of S and T are not necessarily required during the sampling process. By combining all the terms above, we have

$$\begin{aligned} \mathcal{R}_{\mathcal{T}}(h) \leq & \mathcal{R}_{\mathcal{V}}(h) + \sqrt{\frac{4}{n} \left(d \log \frac{2en}{d} + \log \frac{4}{\delta} \right)} + \hat{d}_{\mathcal{H}}(\tilde{S}, T) \\ & + 4 \sqrt{\frac{1}{n} \left(d \log \frac{2n}{d} + \log \frac{4}{\delta} \right)} + \lambda'. \end{aligned} \quad (9)$$

where λ' is analogous to λ and $\lambda' \geq \lambda$ as \tilde{X} is the weighted average of X . Because λ' is determined by \mathcal{S} , \mathcal{T} , and \mathcal{H} , we use the notation $\Omega(\mathcal{S}, \mathcal{T}, \mathcal{H})$ from [59] to replace λ and have (7). \square

Note that we assume that \mathcal{H} is a set of binary classifiers for simplicity. As mentioned in [42], [60], [61], the same analysis holds for multi-class settings.

Given \mathcal{S} and \mathcal{T} , $\mathcal{R}_{\mathcal{T}}(h)$ is determined by $\hat{d}_{\mathcal{H}}(\tilde{S}, T)$, with fixed h , n , and \mathcal{H} . $\hat{d}_{\mathcal{H}}(\tilde{S}, T)$ is hard to define for dense prediction tasks. However, $\hat{d}_{\mathcal{H}}(\tilde{S}, T)$ can be intuitively interpreted as the similarity between \tilde{S} and T . In addition to the minimization of $\mathcal{R}_{\mathcal{V}}(h)$ by gradient descent, we want to make $\hat{d}_{\mathcal{H}}(\tilde{S}, T)$ as small as possible. Because T is a real dataset, the minimization of $\hat{d}_{\mathcal{H}}(\tilde{S}, T)$ is equivalent to generating a realistic \tilde{S} close to T . Based on the assumption of similarity in human anatomical structures, Eq. (3) and Eq. (4) are designed to generate a realistic vicinal distribution. Indeed, an unrealistic \tilde{S} could also increase $\Omega(\mathcal{S}, \mathcal{T}, \mathcal{H})$, which can be viewed as the difficulty of the learning task intuitively. So an ideal \mathcal{V} should have the following properties: 1) \tilde{x} is realistic enough compared to x , and 2) the corresponding \tilde{y} should have semantic meaning.

ACKNOWLEDGMENT

The authors would like to thank Ziyi Chen from Utah University for helpful discussion of Dirichlet distribution and thank Yiliang Jiang from New York University for proofreading. The authors would also like to thank Google for providing the GPU for this study. This work was partially funded by the Norwegian Research Council (302022).

REFERENCES

- [1] J. Long, E. Shelhamer, and T. Darrell, "Fully convolutional networks for semantic segmentation," in *Proceedings of the IEEE Conference on Computer Vision and Pattern Recognition*, 2015, pp. 3431–3440.
- [2] O. Ronneberger, P. Fischer, and T. Brox, "U-net: Convolutional networks for biomedical image segmentation," in *International Conference on Medical Image Computing and Computer-Assisted Intervention*, 2015, pp. 234–241.
- [3] L. Chen, G. Papandreou, I. Kokkinos, K. Murphy, and A. L. Yuille, "DeepLab: Semantic image segmentation with deep convolutional nets, atrous convolution, and fully connected crfs," *IEEE Transactions on Pattern Analysis and Machine Intelligence*, vol. 40, no. 4, pp. 834–848, 2017.
- [4] G. González, G. R. Washko, and R. S. J. Estépar, "Multi-structure segmentation from partially labeled datasets. application to body composition measurements on ct scans," in *Image Analysis for Moving Organ, Breast, and Thoracic Images*. Springer, 2018, pp. 215–224.
- [5] O. Petit, N. Thome, A. Charnoz, A. Hostettler, and L. Soler, "Handling missing annotations for semantic segmentation with deep convnets," in *Deep Learning in Medical Image Analysis and Multimodal Learning for Clinical Decision Support*. Springer, 2018, pp. 20–28.
- [6] Y. Zhou, Z. Li, S. Bai, C. Wang, X. Chen, M. Han, E. Fishman, and A. L. Yuille, "Prior-aware neural network for partially-supervised multi-organ segmentation," in *Proceedings of the IEEE International Conference on Computer Vision*, 2019, pp. 10672–10681.
- [7] X. Fang and P. Yan, "Multi-organ segmentation over partially labeled datasets with multi-scale feature abstraction," *IEEE Transactions on Medical Imaging*, 2020.
- [8] D. Arpit, S. Jastrzebski, N. Ballas, D. Krueger, E. Bengio, M. S. Kanwal, T. Maharaj, A. Fischer, A. Courville, Y. Bengio *et al.*, "A closer look at memorization in deep networks," in *Proceedings of the 34th International Conference on Machine Learning*. JMLR. org, 2017, pp. 233–242.
- [9] C. Zhang, S. Bengio, M. Hardt, B. Recht, and O. Vinyals, "Understanding deep learning requires rethinking generalization," in *International Conference on Learning Representation*, 2017.
- [10] K. Dmitriev and A. E. Kaufman, "Learning multi-class segmentations from single-class datasets," in *Proceedings of the IEEE Conference on Computer Vision and Pattern Recognition*, 2019, pp. 9501–9511.
- [11] O. Chapelle, J. Weston, L. Bottou, and V. Vapnik, "Vicinal risk minimization," in *Advances in Neural Information Processing Systems*, 2001, pp. 416–422.
- [12] H. Zhang, M. Cisse, Y. N. Dauphin, and D. Lopez-Paz, "mixup: Beyond empirical risk minimization," in *International Conference on Learning Representations*, 2018.
- [13] S. Yun, D. Han, S. J. Oh, S. Chun, J. Choe, and Y. Yoo, "Cutmix: Regularization strategy to train strong classifiers with localizable features," in *Proceedings of the IEEE International Conference on Computer Vision*, 2019, pp. 6023–6032.
- [14] J. Shiraishi, S. Katsuragawa, J. Ikezoe, T. Matsumoto, T. Kobayashi, K.-i. Komatsu, M. Matsui, H. Fujita, Y. Kadera, and K. Doi, "Development of a digital image database for chest radiographs with and without a lung nodule: receiver operating characteristic analysis of radiologists' detection of pulmonary nodules," *American Journal of Roentgenology*, vol. 174, no. 1, pp. 71–74, 2000.
- [15] X. Zhuang, K. S. Rhode, R. S. Razavi, D. J. Hawkes, and S. Ourselin, "A registration-based propagation framework for automatic whole heart segmentation of cardiac mri," *IEEE transactions on medical imaging*, vol. 29, no. 9, pp. 1612–1625, 2010.
- [16] X. Zhuang, W. Bai, J. Song, S. Zhan, X. Qian, W. Shi, Y. Lian, and D. Rueckert, "Multiatlas whole heart segmentation of ct data using conditional entropy for atlas ranking and selection," *Medical physics*, vol. 42, no. 7, pp. 3822–3833, 2015.
- [17] A. Iscen, G. Tolias, Y. Avrithis, and O. Chum, "Label propagation for deep semi-supervised learning," in *Proceedings of the IEEE Conference on Computer Vision and Pattern Recognition*, 2019, pp. 5070–5079.
- [18] T. N. Kipf and M. Welling, "Semi-supervised classification with graph convolutional networks," in *International Conference on Learning Representation*, 2017.
- [19] B. Jiang, Z. Zhang, D. Lin, J. Tang, and B. Luo, "Semi-supervised learning with graph learning-convolutional networks," in *Proceedings of the IEEE Conference on Computer Vision and Pattern Recognition*, 2019, pp. 11 313–11 320.
- [20] J. Dong and T. Lin, "Marginan: Adversarial training in semi-supervised learning," in *Advances in Neural Information Processing Systems*, 2019, pp. 10 440–10 449.
- [21] F. Wang and C. Zhang, "Label propagation through linear neighborhoods," *IEEE Transactions on Knowledge and Data Engineering*, vol. 20, no. 1, pp. 55–67, 2007.
- [22] X. Zhu and Z. Ghahramani, "Learning from labeled and unlabeled data with label propagation," Carnegie Mellon University, Tech. Rep. CMU-CALD-02-107, 2002.
- [23] D. Wang, Y. Zhang, K. Zhang, and L. Wang, "Focalmix: Semi-supervised learning for 3d medical image detection," in *Proceedings of the IEEE/CVF Conference on Computer Vision and Pattern Recognition*, 2020, pp. 3951–3960.
- [24] B. Triggs and J. J. Verbeek, "Scene segmentation with crfs learned from partially labeled images," in *Advances in Neural Information Processing Systems*, 2008, pp. 1553–1560.
- [25] N. Natarajan, I. S. Dhillon, P. K. Ravikumar, and A. Tewari, "Learning with noisy labels," in *Advances in Neural Information Processing Systems*, 2013, pp. 1196–1204.
- [26] M. Everingham, L. Van Gool, C. K. Williams, J. Winn, and A. Zisserman, "The pascal visual object classes (voc) challenge," *International Journal of Computer Vision*, vol. 88, no. 2, pp. 303–338, 2010.
- [27] T.-Y. Lin, M. Maire, S. Belongie, J. Hays, P. Perona, D. Ramanan, P. Dollár, and C. L. Zitnick, "Microsoft coco: Common objects in context," in *European Conference on Computer Vision*. Springer, 2014, pp. 740–755.
- [28] M. Cordts, M. Omran, S. Ramos, T. Rehfeld, M. Enzweiler, R. Benenson, U. Franke, S. Roth, and B. Schiele, "The cityscapes dataset for semantic urban scene understanding," in *Proceedings of the IEEE Conference on Computer Vision and Pattern Recognition*, 2016, pp. 3213–3223.
- [29] P. Y. Simard, Y. A. LeCun, J. S. Denker, and B. Victorri, "Transformation invariance in pattern recognition—tangent distance and tangent propagation," in *Neural Networks: Tricks of the Trade*. Springer, 1998, pp. 239–274.

- [30] L. Holmstrom and P. Koistinen, "Using additive noise in back-propagation training," *IEEE Transactions on Neural Networks*, vol. 3, no. 1, pp. 24–38, 1992.
- [31] S.-M. Moosavi-Dezfooli, A. Fawzi, and P. Frossard, "Deepfool: a simple and accurate method to fool deep neural networks," in *Proceedings of the IEEE Conference on Computer Vision and Pattern Recognition*, 2016, pp. 2574–2582.
- [32] N. V. Chawla, K. W. Bowyer, L. O. Hall, and W. P. Kegelmeyer, "Smote: synthetic minority over-sampling technique," *Journal of Artificial Intelligence Research*, vol. 16, pp. 321–357, 2002.
- [33] I. Goodfellow, J. Pouget-Abadie, M. Mirza, B. Xu, D. Warde-Farley, S. Ozair, A. Courville, and Y. Bengio, "Generative adversarial nets," in *Advances in Neural Information Processing Systems*, 2014, pp. 2672–2680.
- [34] Z. Lu, Z. Fu, T. Xiang, P. Han, L. Wang, and X. Gao, "Learning from weak and noisy labels for semantic segmentation," *IEEE Transactions on Pattern Analysis and Machine Intelligence*, vol. 39, no. 3, pp. 486–500, 2016.
- [35] G. Papandreou, L.-C. Chen, K. P. Murphy, and A. L. Yuille, "Weakly- and semi-supervised learning of a deep convolutional network for semantic image segmentation," in *Proceedings of the IEEE International Conference on Computer Vision*, 2015, pp. 1742–1750.
- [36] Z. Huang, X. Wang, J. Wang, W. Liu, and J. Wang, "Weakly-supervised semantic segmentation network with deep seeded region growing," in *Proceedings of the IEEE Conference on Computer Vision and Pattern Recognition*, 2018, pp. 7014–7023.
- [37] C. Redondo-Cabrera, M. Baptista-Ríos, and R. J. López-Sastre, "Learning to exploit the prior network knowledge for weakly supervised semantic segmentation," *IEEE Transactions on Image Processing*, vol. 28, no. 7, pp. 3649–3661, 2019.
- [38] V. Vapnik, *Statistical learning theory*. Wiley, 1998.
- [39] N. Dong, M. Kampffmeyer, X. Liang, Z. Wang, W. Dai, and E. Xing, "Unsupervised domain adaptation for automatic estimation of cardiothoracic ratio," in *International Conference on Medical Image Computing and Computer-Assisted Intervention*, 2018, pp. 544–552.
- [40] N. Dong, M. Xu, X. Liang, Y. Jiang, W. Dai, and E. Xing, "Neural architecture search for adversarial medical image segmentation," in *International Conference on Medical Image Computing and Computer-Assisted Intervention*, 2019, pp. 828–836.
- [41] N. Dong and E. P. Xing, "Domain adaption in one-shot learning," in *Joint European Conference on Machine Learning and Knowledge Discovery in Databases*. Springer, 2018, pp. 573–588.
- [42] S. Ben-David, J. Blitzer, K. Crammer, and F. Pereira, "Analysis of representations for domain adaptation," in *Advances in Neural Information Processing Systems*, 2007, pp. 137–144.
- [43] O. Oktay, E. Ferrante, K. Kamnitsas, M. Heinrich, W. Bai, J. Caballero, S. A. Cook, A. De Marvao, T. Dawes, D. P. O'Regan *et al.*, "Anatomically constrained neural networks (acnns): application to cardiac image enhancement and segmentation," *IEEE Transactions on Medical Imaging*, vol. 37, no. 2, pp. 384–395, 2017.
- [44] A. V. Dalca, J. Guttag, and M. R. Sabuncu, "Anatomical priors in convolutional networks for unsupervised biomedical segmentation," in *Proceedings of the IEEE Conference on Computer Vision and Pattern Recognition*, 2018, pp. 9290–9299.
- [45] H. Kervade, J. Dolz, M. Tang, E. Granger, Y. Boykov, and I. B. Ayed, "Constrained-cnn losses for weakly supervised segmentation," *Medical Image Analysis*, vol. 54, pp. 88–99, 2019.
- [46] C. Szegedy, V. Vanhoucke, S. Ioffe, J. Shlens, and Z. Wojna, "Rethinking the inception architecture for computer vision," in *Proceedings of the IEEE Conference on Computer Vision and Pattern Recognition*, 2016, pp. 2818–2826.
- [47] R. Müller, S. Kornblith, and G. E. Hinton, "When does label smoothing help?" in *Advances in Neural Information Processing Systems*, 2019, pp. 4696–4705.
- [48] W. Dai, N. Dong, Z. Wang, X. Liang, H. Zhang, and E. P. Xing, "Scan: Structure correcting adversarial network for organ segmentation in chest x-rays," in *Deep Learning in Medical Image Analysis and Multimodal Learning for Clinical Decision Support*, 2018, pp. 263–273.
- [49] P. Moeskops, M. Veta, M. W. Lafarge, K. A. Eppenhof, and J. P. Pluim, "Adversarial training and dilated convolutions for brain mri segmentation," in *Deep Learning in Medical Image Analysis and Multimodal Learning for Clinical Decision Support*. Springer, 2017, pp. 56–64.
- [50] K. Chen, D. Zhu, J. Lu, and Y. Luo, "An adversarial and densely dilated network for connectomes segmentation," *Symmetry*, vol. 10, no. 10, p. 467, 2018.
- [51] Z. Han, B. Wei, A. Mercado, S. Leung, and S. Li, "Spine-gan: Semantic segmentation of multiple spinal structures," *Medical Image Analysis*, vol. 50, pp. 23–35, 2018.
- [52] P. Luc, C. Couprie, S. Chintala, and J. Verbeek, "Semantic segmentation using adversarial networks," in *NIPS Workshop on Adversarial Training*, 2016.
- [53] T. Salimans, I. Goodfellow, W. Zaremba, V. Cheung, A. Radford, and X. Chen, "Improved techniques for training gans," in *Advances in Neural Information Processing Systems*, 2016, pp. 2234–2242.
- [54] D. P. Kingma and J. Ba, "Adam: A method for stochastic optimization," in *International Conference on Learning Representation*, 2015.
- [55] K. He, X. Zhang, S. Ren, and J. Sun, "Deep residual learning for image recognition," in *Proceedings of the IEEE Conference on Computer Vision and Pattern Recognition*, 2016, pp. 770–778.
- [56] S. Motiian, Q. Jones, S. Iranmanesh, and G. Doretto, "Few-shot adversarial domain adaptation," in *Advances in Neural Information Processing Systems*, 2017, pp. 6670–6680.
- [57] F. Milletari, N. Navab, and S.-A. Ahmadi, "V-net: Fully convolutional neural networks for volumetric medical image segmentation," in *2016 Fourth International Conference on 3D Vision (3DV)*. IEEE, 2016, pp. 565–571.
- [58] D. Kifer, S. Ben-David, and J. Gehrke, "Detecting change in data streams," in *Proceedings of the 30th International Conference on Very Large Data Bases*, 2004, pp. 180–191.
- [59] Y. S. Abu-Mostafa, M. Magdon-Ismael, and H.-T. Lin, *Learning from data*. AMLBook, 2012.
- [60] Y. Ganin, E. Ustinova, H. Ajakan, P. Germain, H. Larochelle, F. Laviolette, M. Marchand, and V. Lempitsky, "Domain-adversarial training of neural networks," *Journal of Machine Learning Research*, vol. 17, no. 1, pp. 2096–2030, 2016.
- [61] Y. Zhang, T. Liu, M. Long, and M. Jordan, "Bridging theory and algorithm for domain adaptation," in *International Conference on Machine Learning*, 2019, pp. 7404–7413.